Temperature effects on the seismic response in fluid-saturated poroelastic media

*Juan E. Santos * Universidad de Buenos Aires, Facultad de Ingeniería, Instituto del Gas y del Petróleo, School of Earth Sciences and Engineering, Hohai University, Department of Mathematics, Purdue University, Gabriela B. Savioli, Universidad de Buenos Aires, Facultad de Ingeniería, Instituto del Gas y del Petróleo, José M. Carcione, School of Earth Sciences and Engineering, Hohai University, Associate of National Institute of Oceanography and Applied Geophysics, OGS, Trieste, Italy. and Jing Ba, School of Earth Sciences and Engineering, Hohai University*

SUMMARY

We analyze the changes in seismic response in a fluid saturated poroelastic media due to the inclusion of temperature effects in the model. The mathematical model is obtained combining Biot and Lord-Shulman (LS) theories that describe the porous and thermal effects. The model predicts the propagation of four waves: two compressional P waves, one fast and one slow, a thermal wave, and a shear wave. An initial boundary-value problem (IBVP) for the thermo-poroelastic wave equation is formulated and solved by applying the finite-element (FE) method. The FE procedure is formulated for the 1D case on an open bounded interval with absorbing boundary conditions at the artificial boundaries. The procedure discretizes the solid and fluid displacements and the temperature using piecewise linear globally continuous polinomials. The theory is used to study the propagation of the two compressional P waves and the thermal wave. We compare the coupled and uncoupled cases, including and neglecting viscosity. The algorithms may become useful for a better understanding of the behavior of seismic waves in hydrocarbon reservoirs and crustal rocks, because the assumption of isothermal wave propagation is now removed.

INTRODUCTION

The thermoelasticity theory, that combines deformation and temperature, has applications in a variety of fields, such as seismic attenuation, material science and shocks and vibrations Zener (1938); Lifshitz and Roukes (2000); Carcione et al. (2019b). This theory predicts the existence of one S wave and two P waves, an elastic wave and a thermal wave having similar characteristics to the fast and slow P waves of poroelasticity, respectively (Carcione et al. (2019b)). The mathematical models were formulated by Lord and Shulman (LS) (Lord and Shulman, 1967) that derived hyperbolic type differential equations introducing Maxwell-Vernotte-Cattaneo (MVC) relaxation times into the heat equation (Rudgers, 1990). With this formulation they overcame the inconsistences of the solution of the classic parabolic thermoelasticity equations, presented by Biot (1956) for the non-porous case. Rudgers (1990). analyzed the properties of P and T waves as a function of frequency, while Carcione et al. (Carcione et al., 2019a) developed a numerical algorithm for simulating wave propagation in linear thermoelastic media, based on LS theory, and Wang et al. (2020) derived the corresponding Green function.

Thermo-poroelasticity is a relatively recent field. Sharma (2000) and Carcione et al. (2019a) presented the first clear set of differential equations and plane wave analysis. Besides, the latter authors developed a modeling algorithm to compute transient wave fields (seismograms). The theory predicts the propagation and attenuation of four waves, two compressional waves, fast P (P1) and slow Biot P (P2), a slow thermal wave (T), and a shear wave. The two slow waves exhibit diffusive behavior at low frequencies, depending on the viscosity and thermoelasticity constants. The T wave is coupled with both P-waves.The theory assumes that the temperature in the solid and in the fluid is the same. Wei et al. (2020) acquired the corresponding Green function. In these works, the numerical simulation is performed with a direct method to compute the spatial derivatives, namely, the Fourier pseudospectral differential operator (e.g., Carcione (2014)). The development of a new technique, based on the FEM algorithm, will provide a more flexible approach to represent the heterogeneities of the medium and will provide further crosscheck of both algorithms and the physics of wave propagation.

Santos et al. (2021) prove the existence and uniqueness of the Biot/Lord-Shulman formulation in linear thermo-poroelastic isotropic media, with bounded domains under appropriate boundary and initial conditions. The analysis shows the existence of a unique solution, given in terms of displacements of the solid and fluid phases and temperature, and proves its regularity in the space and time variables.

MATHEMATICAL MODEL

We consider a porous medium saturated by a single phase, compressible viscous fluid and assume that the whole aggregate is isotropic. Let θ be increment of temperature above a reference absolute temperature θ_0 for the state of zero stress and strain.

Let $\mathbf{u} = (\mathbf{u}^s, \mathbf{u}^f)$, where $\mathbf{u}^s = (u_i^s)$ and $\mathbf{u}^f = (u_i^f)$ denote the average particle displacement vectors of the solid and relative fluid phase, respectively. Let $\boldsymbol{\varepsilon}(\mathbf{u}^s) = (\varepsilon_{ij}(\mathbf{u}^s))$ and $\boldsymbol{\sigma}(\mathbf{u},\theta) = (\sigma_{ij}(\mathbf{u},\theta))$ be stress tensors of the solid and bulk material, respectively, and $p_f = p_f(\mathbf{u},\theta)$ be the fluid pressure, with associated constitutive relations

$$\sigma_{ij}(\mathbf{u},\theta) = 2\mu\,\varepsilon_{ij}(u^s) + \delta_{ij}(\lambda_u \nabla\cdot\mathbf{u}^s + B\nabla\cdot\mathbf{u}^f - \beta\,\theta), \quad (1)$$

$$p_f(\mathbf{u},\theta) = -B\nabla\cdot\mathbf{u}^s - M\nabla\cdot\mathbf{u}^f + \beta_f\theta. \quad (2)$$

Biot's dynamical equations taking into account temperature

are

$$\rho_b \mathbf{u}^s + \rho^f \mathbf{u}^f - \nabla \cdot \sigma(\mathbf{u}, \theta) = \mathbf{f}^s \qquad (3)$$
$$\rho^f \mathbf{u}^s + g\mathbf{u}^f + \frac{\eta}{\kappa}\mathbf{u}^f + \nabla p_f(\mathbf{u}, \theta) = \mathbf{f}^f,$$

where $\rho_b = (1-\phi)\rho_s + \phi\rho_f$ denotes the mass density of the bulk material, with ϕ, ρ_s and ρ_f denoting the effective porosity and mass densities of the solid grains and fluid, respectively). Also, η is the fluid viscosity, κ the permeability and $g = \frac{S\rho_f}{\phi}$ the tortuosity.

In (1)-(2) , μ is the dry-rock shear modulus, $\lambda_u = \lambda + \alpha^2 M$, $\alpha = 1 - \frac{K_m}{K_s}$, $M = \left(\frac{\alpha-\phi}{K_s} + \frac{\phi}{K_f}\right)^{-1}$, ϕ is the porosity, $B = \alpha\ M, \beta = \beta_m + \beta_f$, with λ_u being the Lamé coefficient of the fluid-saturated frame and K_s, K_m and K_f denoting the bulk moduli of the grains, solid and fluid, respectively. The positive coupling coefficients β_m and β_f are the thermoelasticity coefficients of the frame and fluid, respectively.

On the other hand, the generalized heat equation is (Sharma (2000), Carcione et al. (2019b)):

$$\tau\ c\ \ddot{\theta} + c\ \dot{\theta} - \nabla \cdot (\gamma \nabla \theta) + (1-\phi)\beta_m \theta_0 \nabla \cdot \dot{\mathbf{u}}^s$$
$$+\phi\beta_f \theta_0 \nabla \cdot \dot{\mathbf{u}}^f + \tau(1-\phi)\beta_m T_o \nabla \cdot \ddot{\mathbf{u}}^s \qquad (4)$$
$$+\tau\phi\beta_f T_o \nabla \cdot \ddot{\mathbf{u}}^f = -q.$$

where q is a heat source. Also, $\gamma = (1-\phi)\gamma_m + \phi\gamma_f$ is the bulk coefficient of heat conduction (or thermal conductivity), with γ_m and γ_f being the heat conduction of the frame and the fluid, respectively; $c = (1-\phi)c_m + \phi c_f$ is the bulk specific heat of the unit volume in the absence of deformation and τ is a MVC relaxation time. These equations assume thermal equilibrium between the solid and the fluid, i.e., the temperature in both phases is the same. Thermal equilibrium is valid when the interstitial heat transfer coefficient between the solid and fluid is very large and the ratio of pore surface area to pore volume is sufficiently high. Here, we consider β_m, β_f, γ and c as parameters, obtained from experiments or from a specific theoretical model.

The initial boundary-value problem

The initial boundary-value problem (IBVP) is formulated in an open bounded domain $\Omega \subset R^d$, d=1,2,3 with boundary Γ and a time interval $J = (0,T)$ as follows: find $(\mathbf{u}, \theta)$ satisfying (3) and (4) with initial conditions

$$\mathbf{u}(x,0) = \mathbf{u}^0 = (\mathbf{u}^{0,s}, \mathbf{u}^{0,f}),$$
$$\dot{\mathbf{u}}(x,0) = \mathbf{u}^1 = (\mathbf{u}^{1,s}, \mathbf{u}^{1,f}),$$
$$\theta(x,0) = \theta^0, \quad \dot{\theta}(x,0) = \theta^1,\ x \in \Omega, \qquad (5)$$

and absorbing boundary conditions

$$-\mathscr{G}_\Gamma(\mathbf{u}, \theta) = \mathscr{D}\mathscr{S}(\dot{\mathbf{u}}),$$
$$-\gamma \nabla\theta \cdot \nu = \tau c v_\theta \dot{\theta} \quad x \in \Gamma, \quad t \in J, \qquad (6)$$

where

$$\mathscr{G}(\mathbf{u}, \theta) = \left(\sigma\nu \cdot \nu, \sigma\nu \cdot \chi, p_f\right)(\mathbf{u}, \theta),$$
$$\mathscr{S}(\dot{\mathbf{u}}) = \left(\dot{\mathbf{u}}^s \cdot \nu, \dot{\mathbf{u}}^s \cdot \chi, \dot{\mathbf{u}}^f \cdot \nu\right) \qquad (7)$$

In (6)-(7), ν and χ are the unit vector outer normal and unit vector tangent on Γ oriented counterclockwise. The matrix $\mathscr{D}$ is positive definite and $v_\theta = \sqrt{\gamma/(\tau c)}$ is the heat speed (e.g., Carcione et al.Carcione et al. (2020)).

An existence and uniqueness result for the solution of (3)-(5) with different boundary conditions than those in (6) is given in Santos et al. (2021).

The initial boundary-value problem (3)-(6) was solved in the 1D case using a time-explicit conditionally stable Finite Element (FE) method with linear polynomials to represent the temperature and the solid and fluid displacements.

NUMERICAL RESULTS

The IVBP was solved for the 1D case in an interval $\Omega = (0, L)$, L = 150 m discretized using a uniform mesh with mesh size $h = 0.175$ m and a time step $dt = 7.95 \times 10^{-3}$ ms.

The thermoporoelastic material properties are given in Table 1 Carcione (2014).

Table 1. Material Properties

Grain bulk modulus, K_s	35 GPa
density, ρ_s	2650 kg/m^3
Frame bulk modulus, K_m	1.7 GPa
shear modulus, μ_m	1.885 GPa
porosity, ϕ	0.3
permeability, k	1 darcy
Fluid bulk modulus, K_f	2.4 GPa
density, ρ_f	1000 kg/m^3
viscosity, η_f	0.001 Pa $\cdot$ s
thermoelasticity coefficient, β_f	40000 kg/(m s^2 K)
Bulk specific heat, c	820 kg/(m s^2 K)
thermoelasticity coefficient, β	120000 kg/(m s^2 K)
absolute temperature, T_0	300 K
thermal conductivity, γ	4.5 $\times 10^6$ kg/m^3
relaxation time, τ	1.5 $\times 10^{-2}$ s

The medium is uniform in all experiments, initially at rest with a point dilatational source $\mathbf{f} = (\mathbf{f}^s, \mathbf{f}^s, q)$ on the spatial axis x of time history

$$g(t) = -16 f_0^2 (t - t_0) e^{-8 f_0^2 (t-t_0)^2} \qquad (8)$$

with $t_0 = 1.25/f_0$ and f_0 being the dominant frequency, chosen to be 200 Hz. At this frequency the approximate values of the phase velocities of the P1, P2 and T waves at zero frequency are 2400 m/s, 800 m/s and 500 m/s, respectively.

The source is located at x_s =1 m and temperature and frame and fluid displacements traces are recorded at $x_r = 61$ m.

The experiments consider the uncoupled and coupled Cases considering the vanishing or non-zero coupling coefficients β, β_m and β_f.

Figures 1 and 2 display snapshots of the frame at times 23.5 and 47 ms for the coupled Case and zero viscosity and non-zero viscosities. Figure 1 exhibits clearly the P1, P2 and T

waves as they travel along the domain. On the other hand Figure 2 only shows P1 and T traveling waves, the P2 wave is not observed due to its diffusive behavior.

Figure 3 compares temperature snapshots at time 23.5 and 47 ms for the uncoupled and coupled Cases for non-zero viscosity. The T wave is seen to travel at lower speed and with much higher amplitude in the coupled than the uncoupled Case. Furthermore in the coupled Case the T wave suffer attenuation when traveling in the domain, while the P1 wave is observed to travel with almost no attenuation.

Figures 4 and 5 displays temperature and frame traces for the coupled Case and zero and non-zero viscosity. As expected, for zero viscosity three wave arrivals are observed (red curve) at early times as compared with the non-zero viscosity curves, where only two arrivals can be seen. The T wave is the one with lower amplitude as compared with the P1 and P2 waves.

Finally, Figure 6 shows a frame snapshot at 47 ms for the case when the dilatational source is located only in the frame. The additional slowest wavefront corresponds to a T wave generated due to the coupling of the Biot's and heat equations as defined in (3)–(4)

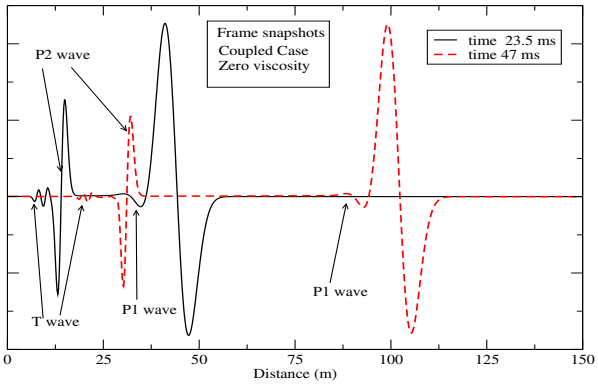

Figure 1: Frame snapshots at 23.5 and 47 ms, coupled Case, zero viscosity experiment.

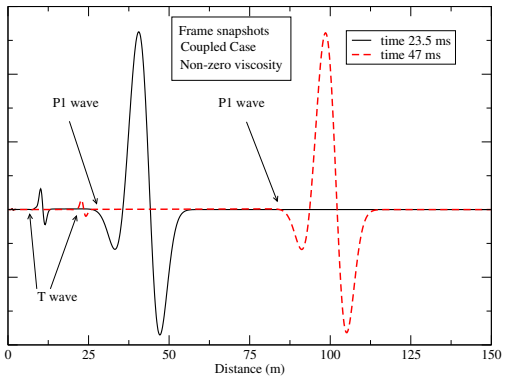

Figure 2: Frame snapshots at 23.5 and 47 ms, coupled Case, non-zero viscosity experiment.

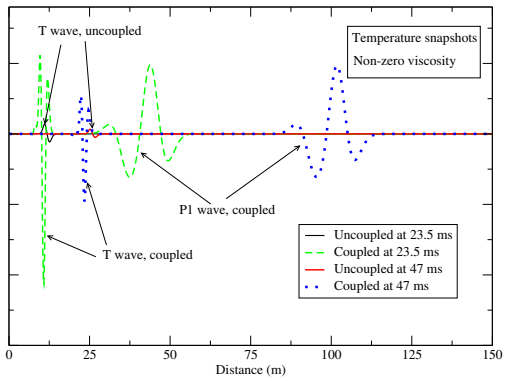

Figure 3: Temperature snapshots, non-zero viscosity experiment. Comparison between uncoupled and coupled Cases at two different times: 23.5 ms and 47 ms.

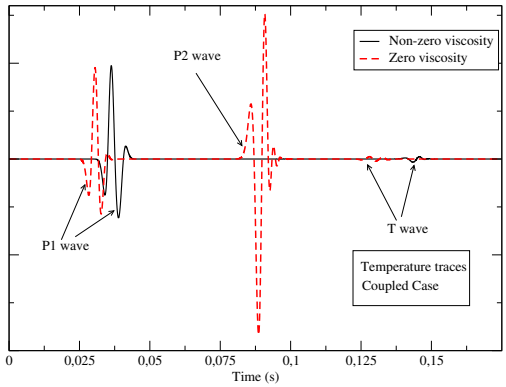

Figure 4: Temperature traces, coupled Case. Comparison between non-zero and zero viscosity experiments.

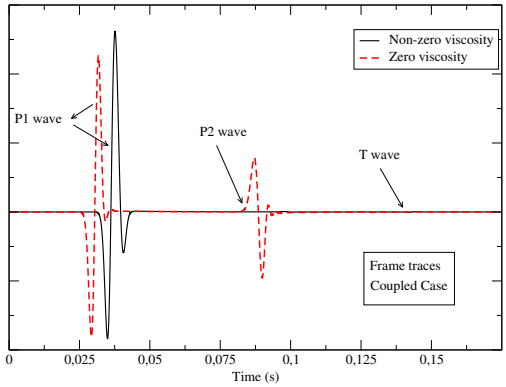

Figure 5: Frame traces, coupled Case. Comparison between non-zero and zero viscosity experiments.

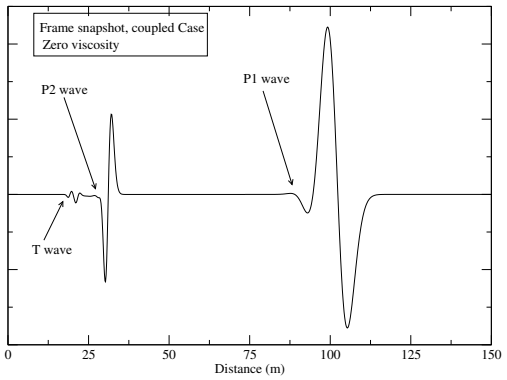

Figure 6: Frame snapshot at 47 ms for zero viscosity, coupled Case. The source is located only in the frame.

CONCLUSIONS

We have presented a time-explicit Finite Element procedure to analyze the propagation of waves in fluid-saturated thermo-poroelastic materials. The examples illustrate the changes in response of the medium when temperature effects are taken into account. The new FE algorithm used in the experiments is time-explicit and permits to solve sequentially the Biot's and heat equation, allowing its simply computational implementation. T waves are coupled with the compresional P1 and P2 waves, inducing additional energy losses not present in the classical Biot model. Furthermore, in the coupled case temperature T waves exhibit higher amplitudes than the compressional waves, suffering attenuation while traveling. Besides, frame sources are seen to induce T waves. Energy losses associated with T waves will be investigated in future research.

ACKNOWLEDGMENTS

This work was partially funded by ANPCyT, Argentina (PICT 2015 1909) and Universidad de Buenos Aires (UBACYT 20020190100236BA)

REFERENCES

Carcione, J. M., 2014, Wave fields in real media. theory and numerical simulation of wave propagation in anisotropic, anelastic, porous and electromagnetic media: Elsevier, Thid edition, extended and revised.

Carcione, J. M., F. Cavallini, E. Wang, J. Ba, and L. Y. Fu, 2019a, Physics and simulation of wave propagation in linear thermoporoelastic media: Journal of Geophysical Research: Solid Earth, **124**, 8147–8166.

Carcione, J. M., D. Gei, J. E. Santos, L. Fu, and J. B. 2, 2020, Canonical analytical solutions of wave-induced thermoelastic attenuation: Geophys. J. Int., https://doi.org/10.1093/gji/ggaa033, **221**, 835–842.

Carcione, J. M., Z. W. Wang, W. Ling, E. Salusti, J. Ba, and L. Y. Fu, 2019b, Simulation of wave propagation in linear thermoelastic media: Geophysics, https://doi.org/10.1190/geo2018-0448.1., **84**, T1, T11.

Lifshitz, R., and M. L. Roukes, 2000, Thermoelastic damping in micro- and nanomechanical systems: Physical Review B, https://doi.org/10.1103/PhysRevB.61.5600., **61**.

Lord, H., and Y. S. Shulman, 1967, A generalized dynamical theory of thermoelasticity: Journal of the Mechanics and Physics of Solids, **15**, 299–309.

Rudgers, A. J., 1990, Analysis of thermoacoustic wave propagation in elastic media: The Journal of the Acoustical Society of America, https://doi.org/10.1121/1.399856, **88**.

Santos, J. E., J. M. Carcione, and J. Ba, 2021, Existence and uniqueness of solutions of thermo-poroelasticity: Journal of Mathematical Analysis and Applications, https://doi.org/10.1016/j.jmaa.2020.124907, **499**.

Sharma, M. D., 2000, Wave propagation in thermoelastic saturated porous medium: Journal of Earth System Science, https://doi.org/10.1007/s12040-008-0080-4, **117**, 951–958.

Zener, C., 1938, Internal friction in solids. ii. theory of internal friction in reeds: Physical Review, **52**, 230–235.